The male germline-specific protein MAPS is indispensable for pachynema progression and fertility

Miao Li[a,b], Jiahuan Zheng[a,b], Gaopeng Li[c], Zexiong Lin[a], Dongliang Li[a], Dongteng Liu[a,b], Haiwei Feng[a,b], Dandan Cao[a], Ernest H. Y. Ng[a,b], Raymond H. W. Li[a,b], Chunsheng Han[d,e,f], William S. B. Yeung[a,b], Louise T. Chow[c,1], Hengbin Wang[c,1], and Kui Liu[a,b,1]

[a]Shenzhen Key Laboratory of Fertility Regulation, Center of Assisted Reproduction and Embryology, The University of Hong Kong–Shenzhen Hospital, 518053 Shenzhen, Guangdong, China; [b]Department of Obstetrics and Gynecology, Li Ka Shing Faculty of Medicine, The University of Hong Kong, Hong Kong, China; [c]Department of Biochemistry and Molecular Genetics, University of Alabama at Birmingham, Birmingham, AL 35294-0024; [d]State Key Laboratory of Stem Cell and Reproductive Biology, Institute of Zoology, Chinese Academy of Sciences, 100101 Beijing, China; [e]Institute for Stem Cell and Regeneration, Chinese Academy of Sciences, 100101 Beijing, China; and [f]University of Chinese Academy of Sciences, Chinese Academy of Sciences, 100049 Beijing, China

Contributed by Louise T. Chow, January 12, 2021 (sent for review December 10, 2020; reviewed by Anders Hofer, Kazuhiro Kawamura, and Mingxi Liu)

Meiosis is a specialized cell division that creates haploid germ cells from diploid progenitors. Through differential RNA expression analyses, we previously identified a number of mouse genes that were dramatically elevated in spermatocytes, relative to their very low expression in spermatogonia and somatic organs. Here, we investigated in detail *1700102P08Rik,* one of these genes, and independently conclude that it encodes a male germline-specific protein, in agreement with a recent report. We demonstrated that it is essential for pachynema progression in spermatocytes and named it male pachynema-specific (MAPS) protein. Mice lacking *Maps* (*Maps*$^{-/-}$) suffered from pachytene arrest and spermatocyte death, leading to male infertility, whereas female fertility was not affected. Interestingly, pubertal *Maps*$^{-/-}$ spermatocytes were arrested at early pachytene stage, accompanied by defects in DNA double-strand break (DSB) repair, crossover formation, and XY body formation. In contrast, adult *Maps*$^{-/-}$ spermatocytes only exhibited partially defective crossover but nonetheless were delayed or failed in progression from early to mid- and late pachytene stage, resulting in cell death. Furthermore, we report a significant transcriptional dysregulation in autosomes and XY chromosomes in both pubertal and adult *Maps*$^{-/-}$ pachytene spermatocytes, including failed meiotic sex chromosome inactivation (MSCI). Further experiments revealed that MAPS overexpression in vitro dramatically decreased the ubiquitination levels of cellular proteins. Conversely, in *Maps*$^{-/-}$ pachytene cells, protein ubiquitination was dramatically increased, likely contributing to the large-scale disruption in gene expression in pachytene cells. Thus, MAPS is a protein essential for pachynema progression in male mice, possibly in mammals in general.

male germline-specific protein | meiosis prophase I | pachynema progression | MAPS

Meiosis is a conserved and specialized form of cell division that produces haploid gametes for sexual reproduction. Meiosis prophase I is a relatively long period during which a series of orderly events occur. Programmed DNA double-strand breaks (DSBs) catalyzed by the topoisomerase-like protein SPO11 are formed at leptonema (1). The DSBs then undergo 3′ end resection to generate 3′ single-stranded DNA overhangs that are protected by the heterotrimeric RPA (replication protein A) complex. This event is followed by loading of the RAD51 recombinase and DNA meiotic recombinase 1 along with other proteins to enable strand invasion into duplex DNA for homolog pairing and recombination intermediate formation (2–4). All DSBs on autosomes are repaired, but only a subset leads to crossovers (5). When autosomes complete synapsis at pachynema, the X and Y chromosomes remain largely unsynapsed and compartmentalized into a nuclear subdomain called the XY body or sex body (6). In response to asynapsis, the X and Y chromosomes are subjected to chromatin modifications leading to transient transcriptional silencing in a process termed meiotic sex chromosome inactivation (MSCI) (6, 7).

Over the past decades, the underlying molecular aspects of meiosis prophase I have been widely studied. Various mutant mouse models have been developed for studying the key events during prophase I progression through the pachytene stage (for reviews, see refs. 8–10). However, the machineries regulating this progression are still not fully understood (11, 12). Transcriptomes during meiosis in males have been reported, but the regulatory factors remain poorly described (13, 14). Nevertheless, epigenetic regulation is thought to be of great importance for the progression of meiosis prophase I, and the role of ubiquitination represents a topic of interest (15–17). For instance, a recent study reported that ubiquitinated proteins localized on the chromosome axis might regulate the stabilization and degradation of recombination factors in order to enable proper synapsis, DSB repair, and crossover formation (16).

Wu et al. (18) have reported that the gene *1700102P08Rik* is specifically expressed in mouse testes, and the knockout male mice were infertile. To identify novel genes regulating meiosis prophase I progression in spermatocytes, we previously

Significance

During meiosis prophase I in mammals, a series of events occur, such as homologous recombination, DSB repair, crossover formation, XY body formation, and meiotic sex chromosome inactivation (MSCI). We report here that a male pachynema-specific (MAPS) protein is essential for prophase I progression in mouse spermatocytes. *Maps* knockout causes the demise of pachytene spermatocytes throughout early to mid- and late pachynema, resulting in male but not female infertility. Moreover, protein ubiquitination was dramatically increased in *Maps*$^{-/-}$ pachytene spermatocytes, likely contributing to the dysregulated global gene expression, including failed MSCI. In summary, MAPS is an indispensable protein for male fertility.

Author contributions: L.T.C., H.W., and K.L. designed research; M.L., J.Z., G.L., Z.L., D. Li, D. Liu, H.F., D.C., H.W., and K.L. performed research; M.L., J.Z., G.L., Z.L., D. Li, D. Liu, H.F., D.C., E.H.Y.N., R.H.W.L., C.H., W.S.B.Y., L.T.C., H.W., and K.L. analyzed data; and M.L., L.T.C., H.W., and K.L. wrote the paper.

Reviewers: A.H., Umeå University; K.K., International University of Health and Welfare School of Medicine; and M.L., Nanjing Medical University.

The authors declare no competing interest.

[1]To whom correspondence may be addressed. Email: ltchow@uab.edu, hbwang@uab.edu, or kliugc@hku.hk.

This article contains supporting information online at https://www.pnas.org/lookup/suppl/doi:10.1073/pnas.2025421118/-/DCSupplemental.

Published February 18, 2021.

performed RNA sequencing of spermatogonia, leptotene/zygotene spermatocytes, pachytene spermatocytes, and round spermatids isolated by bovine serum albumin gradient sedimentation (19, 20). A number of genes were found to be highly expressed in spermatocytes relative to spermatogonia and somatic tissues, including genes, such as *4930432K21Rik/Mamerr* (male meiosis recombination regulator) and *Spdya* (speedy/RINGO cell cycle regulator family, member A), both of which we had further studied (21, 22). In this report, we selected *1700102P08Rik* for detailed analyses and independently concluded that it is a male germline-specific protein. We found that its RNA and protein were primarily expressed in high levels in pachytene spermatocytes. We named this protein MAPS (male pachynema-specific) protein because it is indispensable for the progression of pachynema.

This protein is of 252 amino acids but has no predicted functional domain through analyses by an online protein domain predictor, ThreaDom (23). To investigate its function, we independently knocked out this gene and generated polyclonal antibodies. Indirect immunofluorescence (IF) examination confirms that MAPS protein is expressed specifically during pachynema progression. *Maps* knockout caused pachytene arrest in spermatocytes. The defects occur at different stages during the pachynema progression in pubertal as opposed to adulthood mice. Nonetheless, they all lead to germ cell death and male infertility. Finally, by detailed molecular studies, we showed that $Maps^{-/-}$ spermatocytes exhibited extensive dysregulation in gene expression from both sex chromosomes and autosomes. We conclude that MAPS plays an indispensable role in regulating gene expression during meiosis pachytene progression in male mice. We observed a substantial reduction in ubiquitination when MAPS was ectopically expressed in vitro. Conversely, in $Maps^{-/-}$ spermatocytes, protein ubiquitination was greatly elevated. We propose that alternations in ubiquitination of cellular proteins are likely to have contributed to these changes in gene expression.

Results

***Maps* Is a Testis-Specific Gene That Is Highly Expressed in Meiotic Spermatocytes at the Pachytene Stage.** First, we isolated spermatocytes form pubertal mice PD17 (postnatal day 17) and adulthood PD60–90. Using RT-PCR (reverse transcription polymerase chain reaction) and qRT-PCR (quantitative real-time PCR) targeting exon 1 to exon 3 of *Maps*, we confirmed its high expression in pachytene spermatocytes relative to other stages of sperm development (Fig. 1*A* and *SI Appendix*, Fig. S1*A*). RT-PCR and qRT-PCR analyses also established that *Maps* mRNA (messenger RNA) was specifically expressed in mouse testes but not in embryonic day 17.5 (E17.5) or adult ovaries, nor in other organs (*SI Appendix*, Fig. S1 *B* and *C*).

We generated a polyclonal antibody against MAPS protein. Immunoblots showed that the MAPS protein was present in both nucleus and cytoplasm fractions in mouse testes (*SI Appendix*, Fig. S1*D*). We then conducted indirect IF assay on paraffin sections and again found that MAPS (in red) was not detected in testicular somatic cells, nor in leptotene spermatocytes where diffused γH2AX (phosphorylation of histone H2AX at serine 139, in green) marked DSBs were seen throughout the entire nucleus (Fig. 1*B*, arrowheads). Rather, MAPS was detected in spermatocytes at the pachytene stages (Fig. 1*B*, arrows) when condensed γH2AX signals were found in the XY body area (Fig. 1*J*).

We next performed chromosome spreading to observe chromosomal behaviors throughout meiotic prophase I. We stained MAPS (in green) along with synaptonemal complex protein 3 (SYCP3), which marks chromosome axes (in red), and confirmed that MAPS was not observed in the nuclei of leptotene or zygotene spermatocytes (Fig. 1 *D* and *E*). It was first detected in early pachytene spermatocytes (Fig. 1*F*) with a widespread localization in the whole nuclei, and this pattern persisted to the diplotene stage (Fig. 1 *G–I*). Also, well-defined and condensed MAPS signals were seen in the XY body area from midpachytene to diplotene stage (Fig. 1 *G–I*, dashed circles). Notably, MAPS and γH2AX were colocalized in the XY body (Fig. 1 *J* and *K*, dashed circles). This colocalization can be better visualized in the three-dimensional movie (Movie S1). Collectively, these results suggest that *Maps* is a male-specific gene related to reproduction.

***Maps* Is Essential for Mouse Spermatogenesis and Male Fertility.** The mouse *Maps* gene is located on chromosome 9. The MAPS protein is highly conserved in mice, rats, and humans, and protein sequence comparison showed a 75% identity between mice and humans and 91% identity between mice and rats (*SI Appendix*, Fig. S1*E*). To determine the functional roles of MAPS in germ cells, we used the CRISPR/Cas9 method to generate a *Maps* knockout mouse model by deleting a genomic DNA fragment of 1,841 bp (base pair) spanning exon 3 (*Methods* and *SI Appendix*, Fig. S2*A*). RT-PCR did not detect *Maps* mRNA (Fig. 1*A*, *Top*), and indirect IF did not detect MAPS protein in $Maps^{-/-}$ testis sections (Fig. 1*C*, arrows, arrowheads). Additionally, chromosome spreading confirmed the absence of MAPS in the nuclei of PD35 $Maps^{-/-}$ spermatocytes at the pachytene stage (Fig. 1*L* compared with Fig. 1 *F–H*). Immunoblot analysis also confirmed the absence of MAPS in $Maps^{-/-}$ testes (Fig. 2*A*).

$Maps^{-/-}$ males were sterile, in agreement with the report by Wu et al. (18), and their testes were smaller than those of $Maps^{+/+}$ mice at PD30 and PD67 (Fig. 2*B*). Histological analysis showed that compared with PD28, PD60, and PD90 $Maps^{+/+}$ testes, where various stages of differentiated spermatocytes, round spermatids, and elongated spermatids were seen (Fig. 2 *C*, *E*, and *G*, arrowheads), the most advanced cells found in $Maps^{-/-}$ seminiferous tubules were likely pachytene cells (Fig. 2 *D*, *F*, and *H*, arrows), and no spermatids were observed. At PD90, normal sperms were seen in the epididymides of $Maps^{+/+}$ mice (Fig. 2*I*, arrows), whereas $Maps^{-/-}$ mice showed a complete absence of sperms (Fig. 2*J*).

***Maps* Knockout Causes Pachytene Arrest with Seemingly Intact Synapsis in Pubertal Mice.** To characterize the defects in $Maps^{-/-}$ spermatocytes, we performed chromosome spreading and systematically analyzed prophase I progression using PD30 testes. As the cell cycle progressed from the leptotene to zygotene stage in $Maps^{+/+}$ mice, the signals of SYCP1 (N terminus) started to appear at the midline of the SYCP3-stained axes at zygotene stage (Fig. 2 *K* and *L*, arrow). Autosomes completed synapsis at the pachytene stage (Fig. 2*M*, arrow), and spermatocytes proceeded to the diplotene stage where autosomes began to desynapse (Fig. 2*N*). The $Maps^{-/-}$ spermatocytes exhibited a similar pattern of cell cycle progression from the leptotene to pachytene stage, where the assemblies of N-terminal ends of SYCP1 dimers were observed in zygotene and pachytene spermatocytes (Fig. 2 *P* and *Q*, arrows). However, PD30 $Maps^{-/-}$ spermatocytes failed to proceed to the diplotene stage and remained at the pachytene stage (Fig. 2*Q*).

We quantified the cell cycle progression of pubertal PD30 spermatocytes and found that $Maps^{+/+}$ spermatocytes contained 63% pachytene and 16% diplotene cells, whereas $Maps^{-/-}$ spermatocytes contained only 39% pachytene cells and no diplotene cells (Fig. 3*A*). The percentages of cells in $Maps^{-/-}$ mice at the leptotene (25%) and zygotene (36%) stages were higher than those in $Maps^{+/+}$ mice (8% and 13%, respectively) (Fig. 3*A*). Thus, the meiotic cell cycle progression appeared retarded and arrested at the pachytene stage in pubertal $Maps^{-/-}$ spermatocytes.

***Maps*$^{-/-}$ Spermatocytes in Pubertal Mice Lack Crossover and Exhibit Defective DSB Repair and XY Body Formation.** To determine whether the developmental arrest in $Maps^{-/-}$ spermatocytes was caused by defects in homologous recombination, we next probed

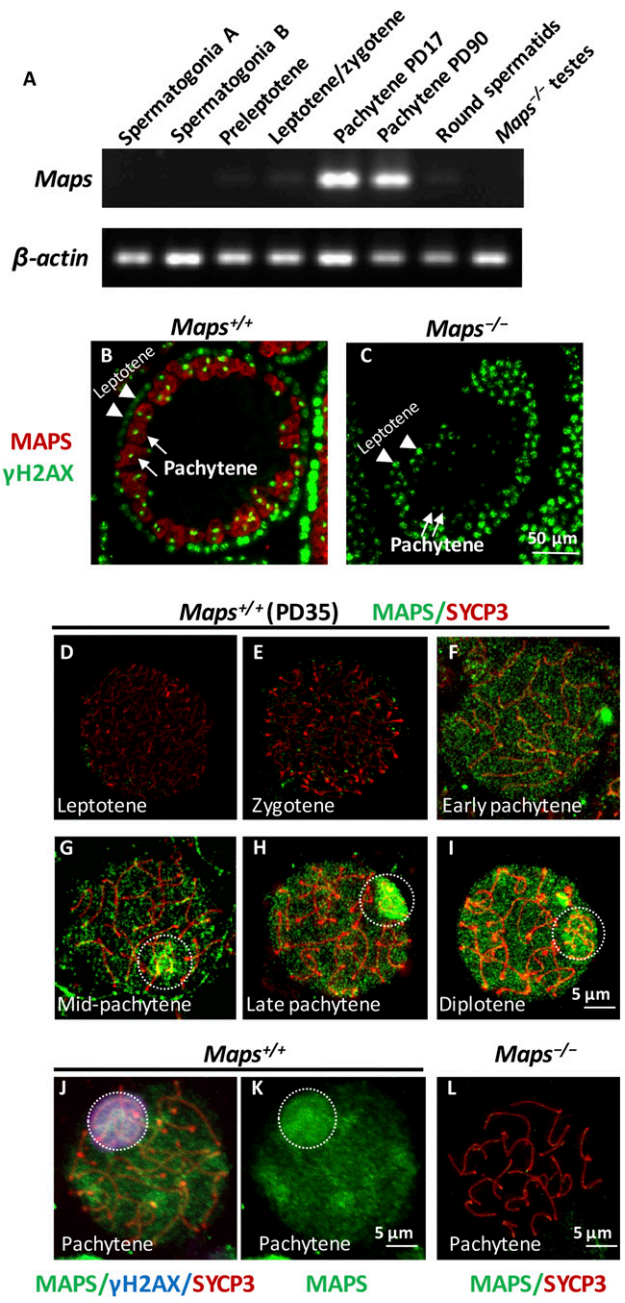

Fig. 1. MAPS expression and localization in meiotic germ cells. (*A*) RT-PCR analysis of *Maps* expression in isolated male germ cells, including two types of spermatogonia (*A* and *B*), preleptotene, leptotene/zygotene, PD17 and PD90 pachytene spermatocytes, and round spermatids, demonstrating that *Maps* was highly expressed in pachytene spermatocytes. $Maps^{-/-}$ testes were negative for *Maps* mRNA. *β-actin* was used as an internal RT-PCR control. (*B* and *C*) IF analysis of MAPS (red) and γH2AX (green) in testis sections from $Maps^{+/+}$ (*B*) and $Maps^{-/-}$ (*C*) mice. MAPS was specifically expressed in pachytene cells (*B*, arrows; with γH2AX accumulated on XY body) but not in leptotene cells (*B*, arrowheads; with γH2AX expressed in the nuclei). MAPS (red) signal was absent in $Maps^{-/-}$ testis sections (*C*), confirming the specificity of the MAPS antibody. (Scale bars, 50 μm.) (*D–I*) chromosome spreads of leptotene to diplotene spermatocytes from PD35 $Maps^{+/+}$ testes stained for MAPS (green) and SYCP3 (red), showing that MAPS was diffusely expressed in the nuclei from early pachytene to diplotene stages (*F–I*), and particularly high signals were seen in the XY body from mid-pachytene to diplotene stages (*G–I*, dashed circles). (Scale bars, 5 μm.) (*J* and *K*) A $Maps^{+/+}$ spermatocyte at late pachytene was stained for MAPS (green), γH2AX (blue), and SYCP3 (red), showing that MAPS colocalized with γH2AX in the XY body (dashed circles). (Scale bars, 5 μm.) (*L*) No MAPS signal was detected in a $Maps^{-/-}$ spermatocyte at pachytene that was stained for MAPS (green) and SYCP3 (red). (Scale bars, 5 μm.)

the distribution of recombination proteins RPA2 and RAD51. We did not find any significant difference in either signals on chromosomes at the zygotene or pachytene stages between $Maps^{+/+}$ and $Maps^{-/-}$ mice (*SI Appendix*, Fig. S2 *B–F* and *G–K*). Thus, the initial recruitment of these proteins was normal in $Maps^{-/-}$ cells.

During recombination, DSBs are repaired by either crossover or noncrossover pathways. We conducted IF assays for MLH1 (mutL homolog 1) (green) and SYCP3 (red) (Fig. 3 *B* and *C*) in PD30 spermatocytes. Compared with $Maps^{+/+}$ pachytene spermatocytes (Fig. 3*B*, marked by arrows, and Fig. 3*D*), there was a complete absence of MLH1 signal in $Maps^{-/-}$ spermatocytes (Fig. 3 *C* and *D*) indicating that crossover did not occur.

In PD30 $Maps^{+/+}$ pachytene cells, autosomes were fully synapsed, and the X and Y chromosomes were paired in the PAR (pseudoautosomal region) to form the XY body (Fig. 3*E*, arrows). We found that 80.2% (85 out of 106 cells) of $Maps^{-/-}$ pachytene spermatocytes exhibited abnormal bivalent XY. We observed 1) asynapsed X and Y chromosomes, with the two chromosomes being far away from each other, representing 6.6% of observed PD30 pachytene cells (7/106) (Fig. 3*F*, arrows); 2) X and Y chromosomes synapsed beyond the PAR, and in some cases, the entire Y chromosome axis synapsed with the X chromosome, representing 27.4% of observed pachytene cells (29/106) (Fig. 3*G*, arrows); and 3) synapsed XY bivalent chromosomes remained extended instead of condensing to form the XY body, representing 46.2% of observed pachytene cells (49/106) (Fig. 3*H*, arrows). We speculated that MAPS may have a function in XY body formation and MSCI. In addition, since pubertal $Maps^{-/-}$ spermatocytes were arrested at early pachytene stage (Fig. 3 *M–R*), the abnormal morphologies of XY chromosomes might also be a result of cell cycle arrest.

At the molecular level, γH2AX signals in $Maps^{+/+}$ pachytene cells disappeared from autosomes but were observed in a well-defined area of the XY body (Fig. 3*I*, dashed circle). In contrast, in most $Maps^{-/-}$ spermatocytes, we observed abnormal γH2AX signals on XY chromosomes. Specifically, the γH2AX signals were poorly defined and irregular in the XY body area (Fig. 3*J*, dashed circle), or as weaker γH2AX signals alongside the XY chromosomes (Fig. 3*K*, dashed circle). Furthermore, the abnormal γH2AX signals were retained on $Maps^{-/-}$ autosomes and were mislocalized as flocs (Fig. 3*J*, arrow) or foci (Fig. 3*L*, arrows). These results strongly support the notion that MAPS is important for proper XY body formation in pachytene spermatocytes in pubertal mice.

***Maps* Deletion Is Associated with the Arrest of Spermatocytes at the Early Pachytene Stage and with Significant Apoptosis in Pubertal Mice.** During meiosis prophase I, pachytene stage lasts the longest and is subdivided into three stages according to the chromosomal behaviors: the "early," "mid-," and "late" pachynema. As XY body was formed at mid-pachytene stage, we speculated that pubertal $Maps^{-/-}$ pachytene spermatocytes were arrested at early pachytene and could not reach mid-pachytene stage. H1t (testis-specific histone variant) is a useful marker for pachytene stage as it became detectable in the entire nuclear region from mid-pachytene stage and increases at late pachytene and diplotene stages (24).

To determine the fate of spermatocytes arrested at the pachytene stage, we performed IF assays on testis sections in PD20 using antibodies against H1t and cleaved-PARP [poly (ADP ribose) polymerase], a marker of apoptosis. In $Maps^{+/+}$ testes, almost all tubules contained many H1t-positive spermatocytes but no apoptotic cells (Fig. 3 *M–O*, arrows). On the contrary, in $Maps^{-/-}$ testes, the spermatocytes expressed very weak H1t signals (Fig. 3 *P* and *R*, arrows), while numerous apoptotic germ cells were seen as indicated by cleaved-PARP signals (Fig. 3 *Q* and *R*, arrows). We concluded that, in young

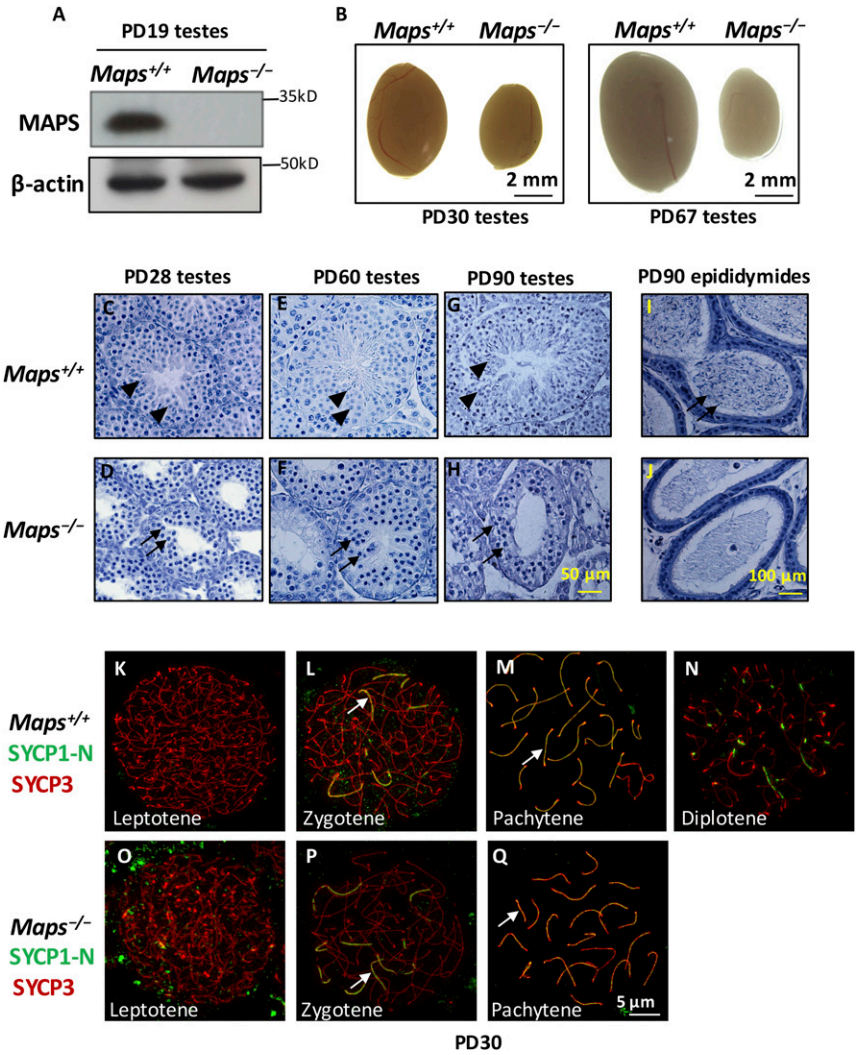

Fig. 2. MAPS is required for mouse spermatogenesis and maintenance of male fertility. (*A*) Immunoblot analysis of MAPS in *Maps*$^{+/+}$ and *Maps*$^{-/-}$ testes, showing that MAPS was absent from PD19 *Maps*$^{-/-}$ testes. β-actin was used as a loading control. (*B*) Testes from PD30 and PD67 *Maps*$^{+/+}$ and *Maps*$^{-/-}$ mice. *Maps*$^{-/-}$ males had reduced testis size. (Scale bars, 2 mm.) (*C*–*H*) Histological analyses of testes from PD28 (*C* and *D*), PD60 (*E* and *F*), and PD90 (*G* and *H*) *Maps*$^{+/+}$ and *Maps*$^{-/-}$ mice. Arrowheads indicate round and elongated spermatids in *Maps*$^{+/+}$ testis, whereas *Maps*$^{-/-}$ spermatocytes were arrested at the pachytene stage (arrows). (Scale bars, 50 μm.) (*I* and *J*) Histological analyses of epididymides from PD90 *Maps*$^{+/+}$ and *Maps*$^{-/-}$ mice. Arrows indicate sperms in *Maps*$^{+/+}$ male, whereas no sperm was observed in *Maps*$^{-/-}$ male. (Scale bars, 100 μm.) (*K*–*Q*) Chromosome spreads of spermatocytes from testes of PD30 *Maps*$^{+/+}$ (*K*–*N*) and *Maps*$^{-/-}$ (*O*–*Q*) males immunostained for SYCP1-N (green) and SYCP3 (red). *Maps*$^{-/-}$ spermatocytes showed seemingly normal synapsis but were arrested at the pachytene stage. Arrows indicate synapsed regions of chromosome axes. (Scale bars, 5 μm.)

pubertal testes, *Maps*$^{-/-}$ spermatocytes were arrested at early pachytene stage and then perished.

Adult *Maps*$^{-/-}$ Spermatocytes Show Normal XY Body Formation and Partly Correct the Defects in Crossover Formation Observed in Pubertal Spermatocytes but Still Exhibit Pachytene Arrest. We compared the percentages of spermatocytes at different stages of prophase 1 progression. In adult (PD60) *Maps*$^{-/-}$ mice, percentages of cells in leptotene, zygotene, and pachytene stages were all higher than those in *Maps*$^{+/+}$ cells (*SI Appendix*, Fig. S3*A*). In contrast, there were only 5% diplotene cells, in comparison to the 39% diplotene cells in the *Maps*$^{+/+}$ mice (*SI Appendix*, Fig. S3 *A*, *E*, and *I*). At PD78, chromosome spreading showed that the synapsis process appeared normal in *Maps*$^{-/-}$ spermatocytes (*SI Appendix*, Fig. S3 *F*–*H*, compared with *SI Appendix*, Fig. S3 *B*–*D* in *Maps*$^{+/+}$ spermatocytes).

We then systematically analyzed the homologous recombination and pachytene progress in adult (PD80) *Maps*$^{-/-}$ and *Maps*$^{+/+}$ mice by staining for RPA2 (*SI Appendix*, Fig. S4 *A*–*G*, in green), RAD51 (*SI Appendix*, Fig. S5 *A*–*G*, in green), and H1t (*SI Appendix*, Figs. S4 *C* and *F* and S5 *C* and *F*, in blue, *SI Appendix*, Figs. S4 *A*, *B*, *D*, and *E* and S5 *A*, *B*, *D*, and *E*, H1t-negative) in adult spermatocytes. We found that the foci numbers and distributions of RPA2 and RAD51 were comparable. H1t signals also appeared similar in *Maps*$^{+/+}$ and *Maps*$^{-/-}$ mid- to late pachytene cells.

For MLH1 staining (Fig. 4 *A* and *B*, in green, arrows), in comparison to around 20 crossover foci in *Maps*$^{+/+}$ pachytene cells, we observed a mean of 13 MLH1 foci in PD130 *Maps*$^{-/-}$ spermatocytes (Fig. 4*C*). Notably, 19.2% of *Maps*$^{-/-}$ spermatocytes (10/52) completely lacked MLH1 signals, 25.0% of *Maps*$^{-/-}$ spermatocytes (13/52) exhibited fewer than 15 MLH1 foci, and only 48.1% of *Maps*$^{-/-}$ spermatocytes (25/52) formed crossovers that were comparable to *Maps*$^{+/+}$ cells. Thus, the defect in crossover formation observed in pubertal *Maps*$^{-/-}$ spermatocytes is partly corrected in adult mice. These observations imply that the meiosis progression is progressively halted during the mid- to late pachytene stage in

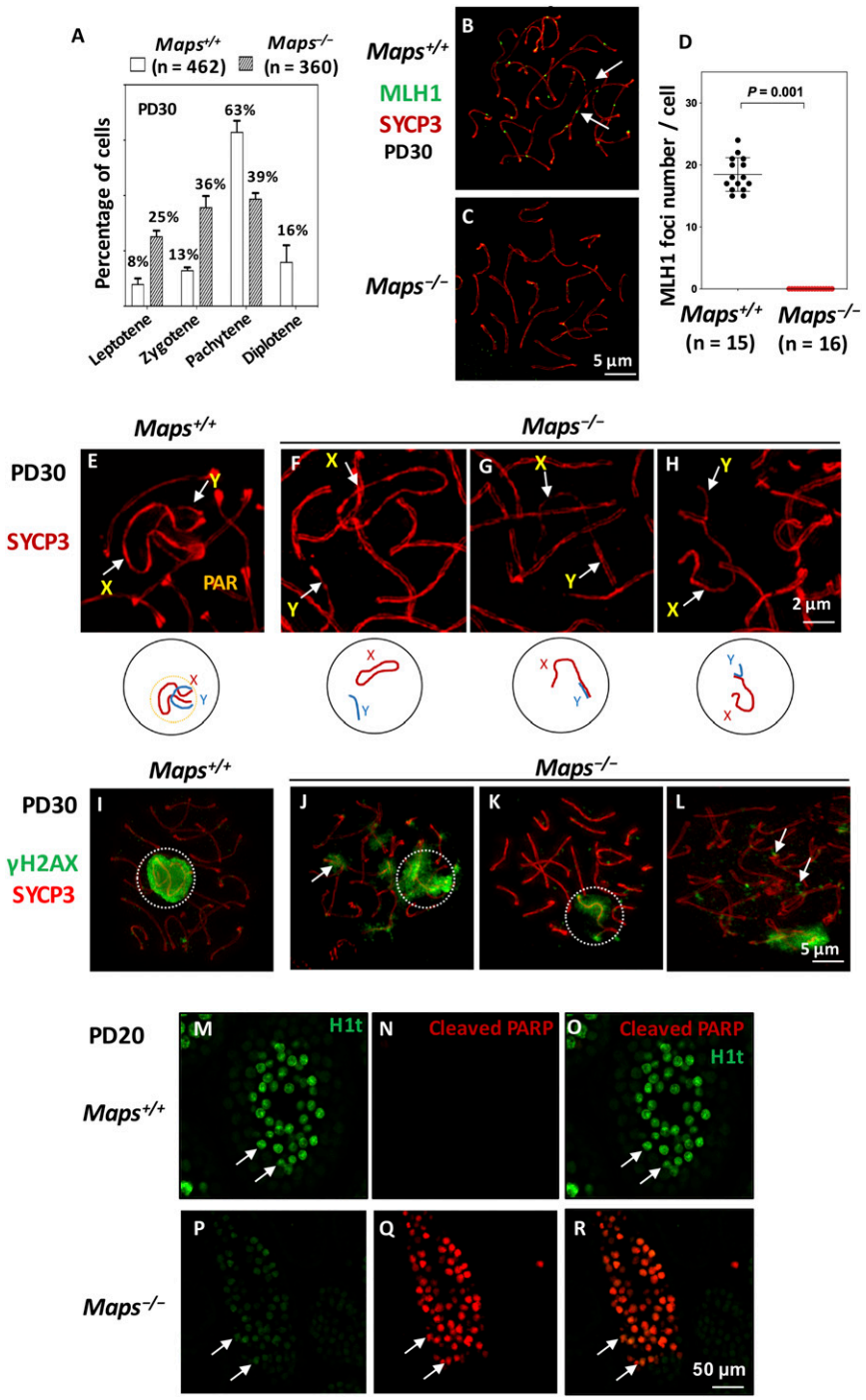

Fig. 3. *Maps* knockout causes pachytene arrest with defective crossover formation, DSB repair, and XY body formation in pubertal mice. (*A*) Analyses of meiotic stages in *Maps*$^{+/+}$ and *Maps*$^{-/-}$ spermatocytes from PD30 testes. $n = 462$ for *Maps*$^{+/+}$ spermatocytes, $n = 360$ for *Maps*$^{-/-}$ spermatocytes. Percentages of cells at indicated meiosis stages were shown. For each genotype, three mice were analyzed. (*B* and *C*) *Maps*$^{+/+}$ and *Maps*$^{-/-}$ spermatocytes immunostained for MLH1 (green, arrows) and SYCP3 (red), showing that *Maps*$^{-/-}$ spermatocytes lack the MLH1 signal. (Scale bars, 5 μm.) (*D*) Scatter plot of MLH1 foci numbers per cell in *Maps*$^{+/+}$ (black) and *Maps*$^{-/-}$ (red) spermatocytes. *Maps*$^{-/-}$ spermatocytes showed no foci of MLH1 (red). Solid lines showed the mean ± SD of foci number in each group of spermatocytes. *P* values were calculated by Student's *t* test. (*E–H*) Chromosome spreads of spermatocytes from testes of PD30 *Maps*$^{+/+}$ (*E*) and *Maps*$^{-/-}$ (*F–H*) males immunostained for SYCP3 (red) with a focus of observing XY bodies (arrows). Based on the morphologies of XY body, cells were classified into four categories, including normal XY body (*E*) where PAR indicates the pseudoautosomal region, XY asynapsis (*F*), XY chromosomes synapse beyond PAR (*G*), and extended X and Y chromosomes (*H*). (Scale bars, 2 μm.) (*I–L*) γH2AX detection in *Maps*$^{+/+}$ (*I*) and *Maps*$^{-/-}$ (*J–L*) pachytene spermatocytes from PD30 testes immunostained for SYCP3 (red) and γH2AX (green), showing abnormal γH2AX signals in sex body area (*J* and *K,* dashed circles), or retained and mislocalized γH2AX signals as flocs or foci on autosomes (*J* and *L*, arrows) of *Maps*$^{-/-}$ spermatocytes. (Scale bars, 5 μm.) (*M–R*) IF analyses of testes from PD20 *Maps*$^{+/+}$ (*M–O*) and *Maps*$^{-/-}$ (*P–R*) males immunostained for cleaved-PARP (red) and H1t (green). H1t signals were strongly positive in *Maps*$^{+/+}$ testes (*M–O,* arrows), and cleaved-PARP signals were observed only in *Maps*$^{-/-}$ spermatocytes (*P–R,* arrows). (Scale bars, 50 μm.)

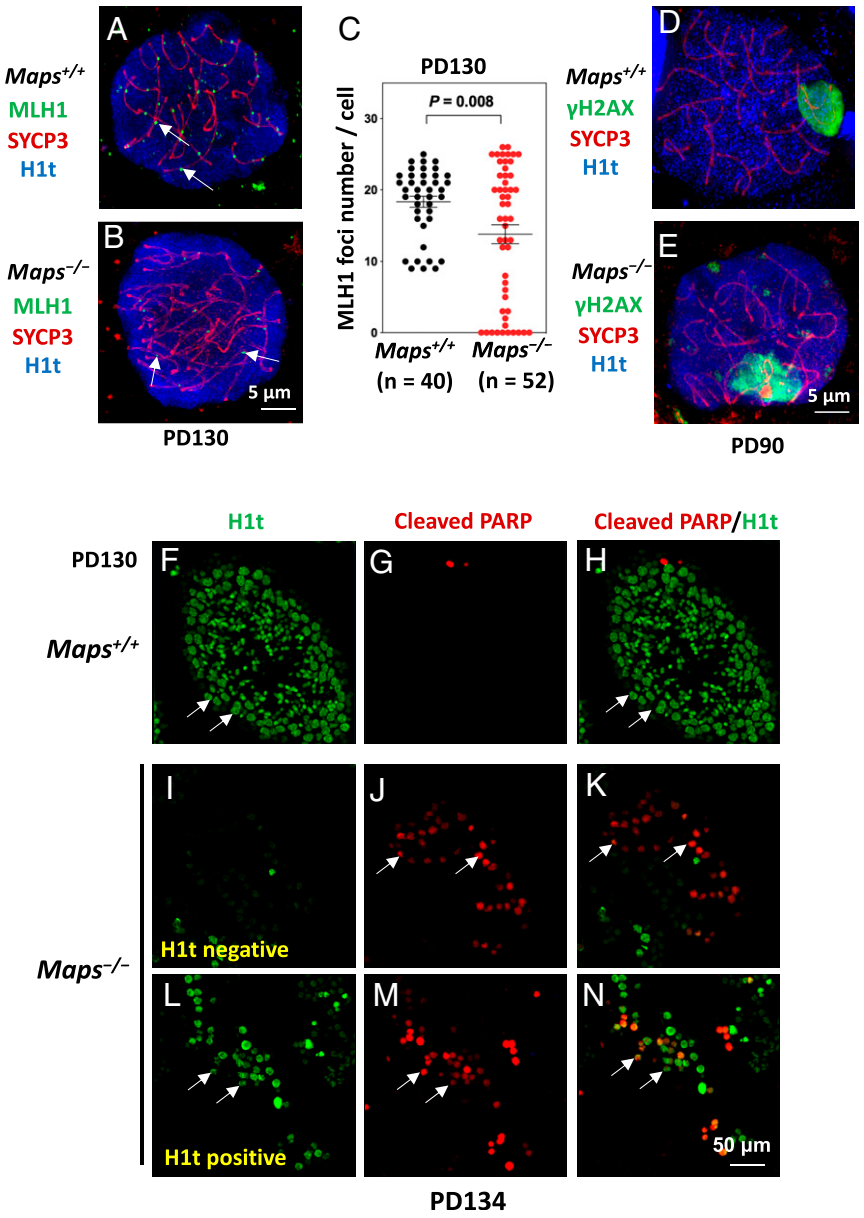

Fig. 4. MAPS deletion is associated with the arrest and apoptosis of spermatocytes at the pachytene stage in adult male testes, with defective crossover but seemingly normal DSB repair and XY body formation. (*A* and *B*) Chromosome spreads of spermatocytes from the testes of PD130 *Maps*$^{+/+}$ and *Maps*$^{-/-}$ mice immunostained for MLH1 (green), SYCP3 (red), and H1t (blue). Representative images are shown. Arrows indicate MLH1 foci on the chromosome axes. (Scale bars, 5 μm.) (*C*) Quantifications of the foci numbers of MLH1 in *Maps*$^{+/+}$ (black dots) and *Maps*$^{-/-}$ (red dots) spermatocytes. Solid lines show the mean ± SD of foci numbers in each group. *P* values were calculated by Student's *t* test. (*D* and *E*) Chromosome spreads of spermatocytes from the testes of PD90 *Maps*$^{+/+}$ and *Maps*$^{-/-}$ mice immunostained for γH2AX (green), SYCP3 (red), and H1t (blue). The XY body with positive γH2AX signals appears normal in *Maps*$^{-/-}$ spermatocytes. Representative images of spermatocytes at the mid- to late pachytene stage are shown. (Scale bars, 5 μm.) (*F–H*) IF analyses from testes of PD134 *Maps*$^{+/+}$ males immunostained for cleaved-PARP (red) and H1t (green). Most cells appeared H1t-positive in the seminiferous tubules (arrows), and apoptosis was rarely observed (arrows). (*I–N*) IF analysis from testes of PD134 *Maps*$^{-/-}$ males immunostained for cleaved-PARP (red) and H1t (green). (*I–K*) Twenty-four percent of *Maps*$^{-/-}$ tubules remained H1t-negative, and these H1t-negative spermatocytes showed signs of apoptosis, with positive cleaved-PARP signals (arrows). (*L–N*) Seventy-six percent of *Maps*$^{-/-}$ tubules contained numerous H1t-positive cells (arrows), and many of these H1t-positive cells also appeared to undergo apoptosis (arrows). (Scale bars, 50 μm.)

Maps$^{-/-}$ spermatocytes. We then examined DSB repair in PD90 pachytene spermatocytes by costaining γH2AX, SYCP3, and H1t. Interestingly, relative to *Maps*$^{+/+}$ cells, in mid- to late *Maps*$^{-/-}$ pachytene cells, the distribution pattern of γH2AX in the sex body was comparable to the wild-type cells (Fig. 4 *D* and *E*).

Adult *Maps*$^{-/-}$ Spermatocytes Undergo Subsequent Apoptosis. Since adult *Maps*$^{-/-}$ spermatocytes develop normal XY bodies, and a fraction of early pachytene cells can progress to mid-pachytene stage, albeit with a delay, then what is the cause for male infertility? To address this question, we performed IF assay to assess H1t and cleaved-PARP staining patterns on paraffin-embedded sections of PD134 testes. In *Maps*$^{+/+}$ testes, most cells appeared H1t-positive in the seminiferous tubules (14/14) (Fig. 4 *F* and *H*, arrows), and apoptosis was rarely observed (Fig. 4 *G* and *H*, arrows). In *Maps*$^{-/-}$ testes, however, around 24% seminiferous tubules observed (6/25) appeared H1t-negative (Fig. 4 *I* and *K*), suggesting that a fraction of early

pachytene cells were still arrested in adult mice. For these tubules, many H1t-negative spermatocytes showed signs of apoptosis, being positive for the cleaved-PARP (Fig. 4 *J* and *K*, arrows). Although 76% of tubules (19/25) contained numerous H1t-positive cells (Fig. 4 *L* and *N*, arrows), many of these cells also appeared to undergo apoptosis, as suggested by the colocalized cleaved-PARP (Fig. 4 *M* and *N*, arrows).

Adult *Maps*$^{-/-}$ Pachytene Spermatocytes Exhibit Retarded Progression from Early to Mid- and Late Pachynema. To investigate why the defects in *Maps*$^{-/-}$ spermatocytes occur at different phases of pachytene progression in pubertal and adult mice, we systematically examined pachytene progression in *Maps*$^{+/+}$ and *Maps*$^{-/-}$ mice of different age. We used H1t expression as a valid marker for progression from early to mid- and late pachynema. We found that in *Maps*$^{+/+}$ pachytene cells, at PD17, 70.0% of the cells were H1t-positive. This proportion increased to 81.0% in PD30 and 82.0% in PD40 (Fig. 5*A*), and to 88.4% in PD50–80 (Fig. 5*A*), while H1t-negative cells correspondingly decreased. Spermatogenesis is a progressive process from spermatogonia to elongated spermatids in waves throughout the reproductive lifetime in male mice, and there exist different waves and stages of spermatocytes in different seminiferous tubules of the same testis, including cells at early pachytene stage (H1t-negative), and mid- to late pachytene cells (H1t-positive) (25, 26). Therefore, although all pachytene cells in *Maps*$^{+/+}$ mice would eventually reach late pachytene stage (i.e., H1t-positive), they would do so in an unsynchronized manner (25, 26). Thus, starting from PD17 onwards, the majority of the first-wave pachytene spermatocytes had reached mid-pachytene stage.

In sharp contrast, very few H1t-positive (i.e., mid-pachytene) spermatocytes were found in PD17, PD30, and PD40 *Maps*$^{-/-}$ testes (Fig. 5*B*); they eventually reached 33.4% in PD50–80 (Fig. 5*B*). These observations indicate that MAPS plays a significant role in driving the transition from early pachynema to mid-pachynema for the first wave of meiosis.

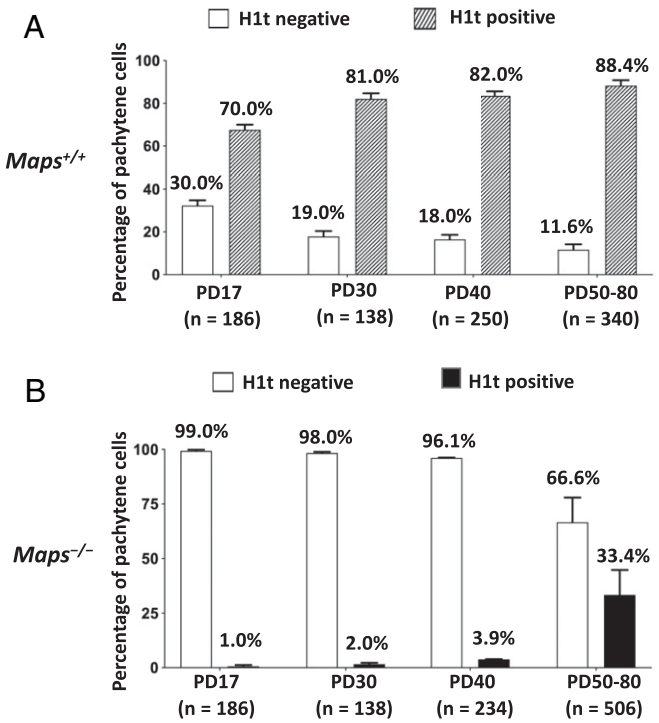

Fig. 5. Adult *Maps*$^{-/-}$ pachytene spermatocytes exhibit retarded progression from early to mid- and late pachynema. (*A* and *B*) Percentages of H1t-negative and H1t-positive pachytene spermatocytes from testes of *Maps*$^{+/+}$ (*A*) and *Maps*$^{-/-}$ (*B*) mice at a range of ages. The numbers of total cells counted were also indicated. The white bars indicate the percentages of H1t-negative cells, and the striped (*A*) or black bars (*B*) indicate the percentages of H1t-positive cells. For each genotype and age, at least three mice were analyzed.

Female *Maps*$^{-/-}$ Mice Have Normal Meiosis Prophase I Progression and Fertility. We also performed chromosome spreading with E17.5 ovaries and found that *Maps*$^{-/-}$ female germ cells formed normal synaptonemal complexes relative to *Maps*$^{+/+}$ cells (*SI Appendix*, Fig. S6 *A–F*), and neither expressed MAPS protein (*SI Appendix*, Fig. S6 *G–J*). Also, crossovers in prophase I of *Maps*$^{-/-}$ female germ cells were normal, with comparable MLH1 foci to *Maps*$^{+/+}$ pachytene cells (*SI Appendix*, Fig. S6 *K* and *L*, arrows). These results confirm that MAPS is not involved in female meiosis prophase I. Indeed, the fertility of *Maps*$^{-/-}$ females was normal.

***Maps*$^{-/-}$ Spermatocytes Fail to Establish MSCI at Both Pubertal and Adult Ages due to Transcription Dysregulation of Sex Chromosomes.** To investigate the underlying mechanisms for pachytene arrest in *Maps*$^{-/-}$ spermatocytes, we isolated pachytene cells from *Maps*$^{+/+}$ and *Maps*$^{-/-}$ testes of PD17 and PD90 mice and performed RNA-sequencing analyses.

In PD17, 89.0% (483 out of 543) of the X-linked protein-coding genes and 86.7% (13 out of 15) of the Y-linked protein-coding genes were differentially expressed between *Maps*$^{-/-}$ and *Maps*$^{+/+}$ pachytene spermatocytes (Table 1 and *SI Appendix*, Fig. S7*A*). For the X chromosome, 89.6% of the differentially expressed genes (433 out of 483) were up-regulated in *Maps*$^{-/-}$ spermatocytes, and for the Y chromosome, all of the genes (13 out of 13) were up-regulated in *Maps*$^{-/-}$ spermatocytes. The median expression of genes from the X and Y chromosomes in *Maps*$^{-/-}$ cells relative to *Maps*$^{+/+}$ cells was increased by a mean of 1.7-fold and 2.1-fold, respectively.

In PD90 pachytene spermatocytes, 98.3% (455 out of 463) of the X-linked protein-coding genes and 100% (6 out of 6) of the Y-linked protein-coding genes were differentially expressed between *Maps*$^{-/-}$ and *Maps*$^{+/+}$ testes (Table 1 and *SI Appendix*, Fig. S7*B*). Of the differentially expressed X chromosome genes, 96.9% (441 out of 455) were up-regulated in *Maps*$^{-/-}$ spermatocytes. One hundred percent (6 out of 6) of the differentially expressed Y chromosome genes were up-regulated in *Maps*$^{-/-}$ spermatocytes. Notably, 389 up-regulated and 11 down-regulated genes overlapped between the PD17 and PD90 groups (*SI Appendix*, Fig. S7 *C* and *D*), implying a common mechanism that regulates the transcription of the X and Y chromosomes. These data indicate that MSCI establishment in *Maps*$^{-/-}$ spermatocytes was significantly disrupted and that MAPS may contribute to the initiation and maintenance of MSCI on X and Y chromosomes.

***Maps*$^{-/-}$ Pachytene Spermatocytes Exhibit Dysregulation in Autosomal Gene Transcription.** Substantial dysregulation of autosomal transcription was also observed in *Maps*$^{-/-}$ pachytene cells relative to *Maps*$^{+/+}$ pachytene cells. In PD17, 68.0% (8,349 out of 12,262) autosomal genes were differentially regulated, among which, 42.0% (3,509 out of 8,349) genes were significantly up-regulated and 58.0% (4,840 out of 8,349) genes were significantly down-regulated in *Maps*$^{-/-}$ cells (Table 1 and *SI Appendix*, Fig. S8*A*). Of the genes with expression levels changed over eightfold, 1,808 genes were down-regulated and only 54 genes were up-regulated, suggesting a large-scale suppression of autosomal gene expression. In PD90 *Maps*$^{-/-}$ pachytene spermatocytes, 89.8% (10,669 out of 11,887) genes on autosomes were differentially regulated (Table 1 and *SI Appendix*, Fig. S8*B*). Among them, 50.9% (5,434 out of 10,669) was up-regulated and 49.1% (5,235 out of 10,669) was down-regulated in *Maps*$^{-/-}$ cells. The analyses also revealed that 3,062 up-regulated and 4,359 down-regulated genes overlapped between the PD17 and PD90 groups (*SI Appendix*, Fig. S8 *C* and

Table 1. Differentially expressed (DE) genes in *Maps*$^{-/-}$ vs. *Maps*$^{+/+}$ spermatocytes

	Chromosomes	DE genes/total genes		Total	Over 2 folds	Over 4 folds	Over 8 folds	Over 16 folds
PD17	X	483/543	Up	433	417	144	6	2
			Down	50	48	47	45	42
	Y	13/15	Up	13	13	7	2	/
			Down	/	/	/	/	/
	Autosome	8,349/12,262	Up	3,509	2,698	854	54	7
			Down	4,840	4,702	2,588	1,808	1,333
PD90	X	455/463	Up	441	441	428	363	125
			Down	14	13	12	10	7
	Y	6/6	Up	6	6	6	6	1
			Down	/	/	/	/	/
	Autosome	10,669/11,887	Up	5,434	4,273	2,958	1,525	350
			Down	5,235	3,929	2,331	1,239	431

The numbers of DE and total genes and up-regulated and down-regulated genes in isolated pachytene spermatocytes from PD17 and PD90 *Maps*$^{-/-}$ mice relative to *Maps*$^{+/+}$ mice were listed. Only protein-coding genes having an average FPKM (fragments per kilobase million) > 1 in either *Maps*$^{+/+}$ or *Maps*$^{-/-}$ group were included. The / indicates 0.

D), suggesting that MAPS regulates autosomal transcription through a similar mechanism in pubertal and adult pachytene spermatocytes.

Importantly, gene ontology analysis showed that, at both PD17 and PD90, genes of the male gamete generation pathway and spermatogenesis pathway were at the top of down-regulated populations (*SI Appendix*, Fig. S9 *A* and *B*).

MAPS Regulates Cellular Protein Ubiquitination In Vitro and In Vivo. Protein ubiquitination is an important posttranslational modification marking proteins for degradation or functional alternation. Ubiquitin can be conjugated to substrate proteins either as monoubiquitination or polyubiquitination. Monoubiquitination is the addition of one ubiquitin molecule to substrates (27), altering its function. Polyubiquitination refers to the addition of a chain of ubiquitin moiety to a residue of substrate protein. The most prominent polyubiquitination through lysine 48 linkage marks the protein for degradation by proteasomes (28). Previous reports suggested that ubiquitin localizes on the axis along surface-spread chromosomes and ubiquitination may regulate synapsis, DSB repair, recombination, and crossover formation through stabilization and degradation of recombination factors (16). In this study, we used FK2 antibody, which recognizes both mono- and poly-ubiquitin conjugates (29), to detect the levels of ubiquitination of cellular proteins.

To determine whether MAPS levels affect cellular protein ubiquitination, we ectopically expressed MAPS-GFP (green fluorescent protein) or MAPS-HA (human influenza hemagglutinin) fusion proteins in transformed human embryonic kidney (HEK) 293T cells that were negative for MAPS. As in pachytene spermatocytes, MAPS-GFP is localized in both nuclei and cytoplasm (Fig. 6*A*). Immunoblots with FK2 antibody revealed that the levels of ubiquitination of cellular proteins were dramatically reduced in MAPS-expressing cells (Fig. 6 *B* and *C* and *SI Appendix*, Fig. S10*A*). Interestingly, the levels of ubiquitinated H2A, a prominent target of monoubiquitination modification, likely represented by the bands around 20 kD, were not obviously affected. This result is better discerned by fractionation of MAPS-expressing cells into soluble and pellet (chromatin-associated proteins) fractions. Immunoblots for FK2 antibody revealed that the levels of ubiquitinated proteins were dramatically reduced in chromatin fractions of MAPS-expressing cells. Immunoblots with HA antibody revealed that MAPS-HA is predominately localized in the soluble fractions with little in the chromatin fractions (Fig. 6*D* and *SI Appendix*, Fig. S10*B*).

To investigate the mechanism by which MAPS affects cellular protein ubiquitination, we tested whether MAPS associates with chromatin. We transfected HeLa cell line expressing Flag-H2B with the MAPS-HA expressing plasmid. Although chromatin was efficiently immunoprecipitated in the pellet fraction by anti–Flag-H2B immunoprecipitation, MAPS (MAPS-HA) was not detected in the immumoprecipitates (Fig. 6*E* and *SI Appendix*, Fig. S10*C*). We then transfected the MAPS-GFP expressing plasmid into HeLa cell line, which stably expresses HA-Cullin 4A (Cul4A), a component of a Cullin family ubiquitin ligase complex that has both cytoplasmic and nuclear substrates (30, 31). We did not find an association between MAPS-GFP with HA-Cul4A by coimmunoprecipitation (Fig. 6*F* and *SI Appendix*, Fig. S10*D*). These results indicate that MAPS does not stably bind to chromatin-associated substrates and did not interact directly with the ubiquitin ligase investigated.

The in vitro data led us to probe for ubiquitinated proteins in pachytene spermatocytes from *Maps*$^{+/+}$ and *Maps*$^{-/-}$ mice. As in HEK 293T cells, MAPS expression was primarily observed in soluble fractions of pachytene spermatocytes, but not in chromatin-associated protein (pellet) fractions (Fig. 7*A*). Histone H3 was used as a marker for chromatin fractions. Immunoblots with FK2 antibody showed that the levels of ubiquitination of cellular proteins were dramatically increased in *Maps*$^{-/-}$ cells relative to *Maps*$^{+/+}$ cells, except that a low-molecular-weight band at around 17 kD showed decreased levels (Fig. 7*B*). These data are in accordance with our in vitro studies (Fig. 6 *B* and *D*) and demonstrate that MAPS regulates cellular protein ubiquitination.

Discussion

During meiosis prophase I in mouse spermatocytes, the pachytene stage lasts for about 6 d (32). Prominent features of pachytene spermatocytes are established at mid-pachynema, including the crossover formation, the formation of the XY body, and MSCI (8–10). In this work, we have identified a male germline-specific protein MAPS, which is essential for the pachynema progression in meiosis prophase I in mice. Knockout of *Maps* causes a progressive cessation of progression from early to mid- and late pachynema in spermatocytes, leading to cell demise and male infertility.

In pubertal *Maps*$^{-/-}$ pachytene spermatocytes, spermatocytes were arrested at early pachytene stage with defective DSB repair, lack of crossovers, and defective XY body formation. However, in adult *Maps*$^{-/-}$ mice, there was seemingly normal DSB repair and normal formation of the XY body, but crossover formation was somewhat defective, and the progression of pachynema was delayed or arrested. Eventually, a fraction of spermatocytes reached the mid- or late pachytene stage. Regardless, spermatocyte demise was a common fate for both pubertal and adult

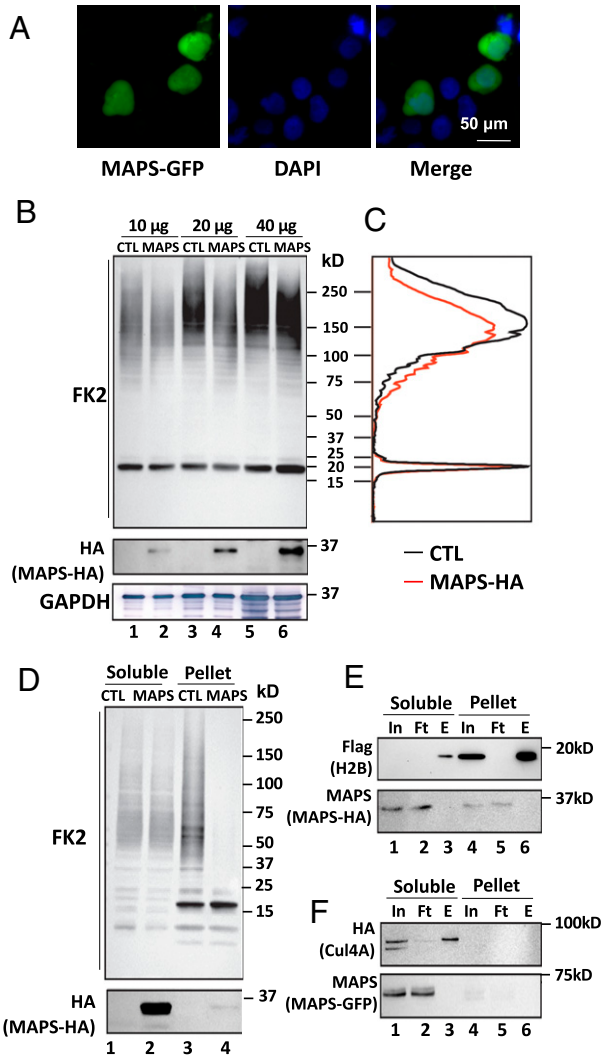

Fig. 6. MAPS regulates cellular protein ubiquitination in vitro. (*A*) Subcellular localization of MAPS. HEK 293T cells were transfected with a MAPS-GFP expression vector and observed by fluorescent microscopy. Nuclei were stained with DAPI. (Scale bars, 50 μm.) (*B*) Ectopic overexpression of MAPS reduces cellular ubiquitination levels. HEK 293T cells were transfected with a MAPS-HA expression vector or an empty control vector (CTL), and total cellular lysates were analyzed by immunoblots using antibodies FK2 (first panel) to detect ubiquitinated proteins, HA (second panel) to detect MAPS-HA overexpression, and GAPDH (third panel) to show equal loading. (*C*) Quantification of changes in protein ubiquitination of cells overexpressing MAPS-HA. Analyses were conducted on *B* loaded with 20 μg of total protein. (*D*) Effects of MAPS-HA overexpression on ubiquitinated proteins in chromatin and soluble fractions. Immunoblots for FK2 antibody revealed that the levels of ubiquitinated proteins were dramatically reduced in chromatin fractions of MAPS-expressing cells. Immunoblots with HA antibody revealed that MAPS-HA is predominately localized in the soluble fractions and little in the chromatin fractions. (*E*) MAPS is not associated with chromatin. A stable HeLa cell line, which expresses Flag-H2B, was transfected with an expression vector of MAPS-HA. The lysates were separated as soluble and chromatin fractions. Anti-Flag immunoprecipitation was used to purify the chromatin. Proteins in In (input), Ft (flow through), and E (eluate) were then immunoblotted with Flag (*Top*) or MAPS (*Bottom*) antibodies. MAPS-HA largely remained in the soluble fractions. (*F*) HeLa cells stably expressing HA-Cul4A were transfected with an MAPS-GFP expressing plasmid. Cul4-DDB-ROC1 complex was purified by anti-HA immunoprecipitation. Immunoblots revealed that MAPS (MAPS-GFP) does not physically associate with the ubiquitin ligase. Parallel gels for *B*, *D*, *E*, and *F* stained with Coomassie brilliant blue to demonstrate equal loading are shown in *SI Appendix*, Fig. S10.

Maps$^{-/-}$ mice. Collectively, these results suggest that MAPS did not seem to be directly involved in the homologous recombination process. Rather, *Maps* deficiency retards and arrests pachytene progression, resulting in cell death.

It should be mentioned that we also generated a *Maps* knock-in mouse model in the *Maps*$^{-/-}$ background. The mice overexpressed HA-tagged MAPS and restored spermatogenesis (see *SI Appendix*, *Methods*). These results rule out any off-target effects during the generation of the *Maps*$^{-/-}$ mice.

It is worth noting that the observed wide range of defects in pachytene progression in *Maps*$^{-/-}$ spermatocytes are distinguishable from the previously reported mutant mouse models with pachytene arrest caused by defects in certain single events. For example, deletion of *Mlh1* caused crossover deficiency and resulted in pachytene arrest (33). *H2ax*$^{-/-}$ and *Mdc1*$^{-/-}$ (mediator of

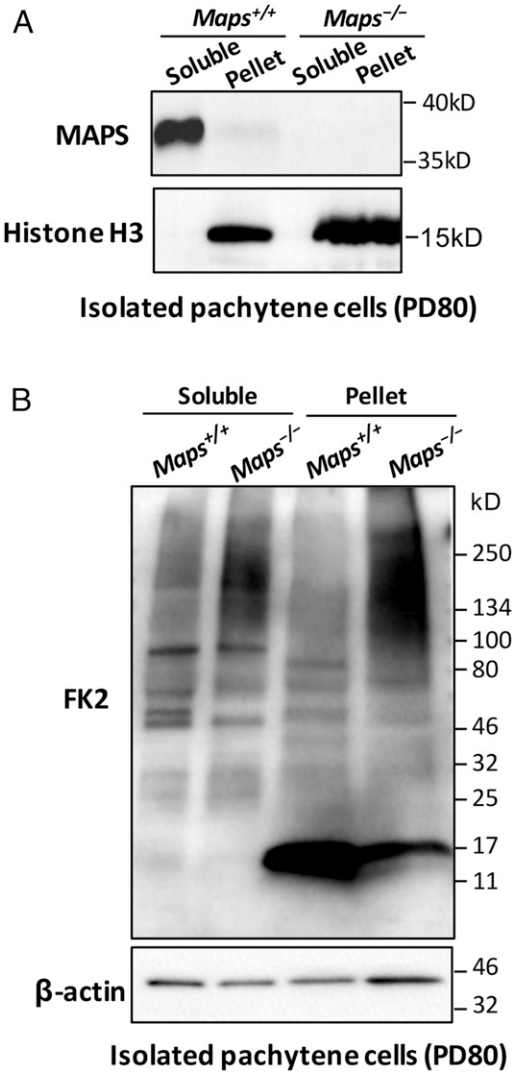

Fig. 7. MAPS regulates cellular protein ubiquitination in pachytene spermatocytes. (*A*) Immunoblots of MAPS in soluble and pellet (chromatin-associated proteins) fractions of isolated pachytene spermatocytes from *Maps*$^{+/+}$ and *Maps*$^{-/-}$ males at PD80, indicating MAPS was primarily present in soluble fractions and only in *Maps*$^{+/+}$ cells. (*B*) Immunoblot analysis of ubiquitinated proteins using antibody FK2 in isolated pachytene spermatocytes from PD80 *Maps*$^{+/+}$ and *Maps*$^{-/-}$ mice. Cellular proteins in *Maps*$^{-/-}$ pachytene spermatocytes have elevated levels of ubiquitination. β-actin was used as a loading control.

DNA damage checkpoint 1) spermatocytes showed mid-pachytene arrest caused by a failure in XY body formation (34, 35).

Our results of the global dysregulation of gene expression from autosomes and sex chromosomes in *Maps*$^{-/-}$ spermatocytes were extraordinary. In particular, genes related to male gamete generation and spermatogenesis pathway were dramatically down-regulated. These striking transcriptional changes are likely the reasons for the observed phenotypes, including the defects in DSB repair, crossover, sex body formation, and MSCI in the pubertal and adult *Maps*$^{-/-}$ spermatocytes, ultimately leading to male infertility. The scale and magnitude of changes are distinct from previous mutant mouse models with MSCI defects, such as mice deficient in *H2ax* (*H2ax*$^{-/-}$) (34), *Mdc1* (*Mdc1*$^{-/-}$) (35) and mice with meiotic deletion of *Setdb1* (SET domain, bifurcated 1) (36), where only expression of a small number of autosomal genes was altered.

The underlying mechanisms for the demise of *Maps*$^{-/-}$ spermatocytes in adult and pubertal mice are similar, as indicated by the large number of overlapping perturbed gene transcription in pubertal and adult *Maps*$^{-/-}$ mouse spermatocytes. The slightly different phenotypes observed in pubertal and adult *Maps*$^{-/-}$ mice may be attributed to differences in the first wave of pubertal spermatogenesis and the adult steady-state spermatogenesis (37). The first wave of spermatocytes comes from NGN-3 (neurogenin-3)-negative differentiating spermatogonia derived from a particular subset of gonocytes in the prepubertal testes. In contrast, spermatocytes in adults are cells differentiated from NGN-3–positive, undifferentiated self-renewing spermatogonia (38). Also, there are known differences in recombination and crossover maturation between the pubertal waves of spermatogenesis and the adult waves (39). In this study, the pubertal spermatocytes seem more vulnerable to the absence of MAPS and were immediately arrested at early pachynema. In adult *Maps*$^{-/-}$ spermatocytes, although some of these cells can progress to late pachytene stage, or even diplotene stage, most of them appear to be lost to apoptosis.

In our first effort to shed light on the mechanism that mediates MAPS function, we expressed MAPS ectopically in cultured cells. We observed that cellular ubiquitination was dramatically reduced. These in vitro observations suggest that MAPS may also affect cellular protein ubiquitination in pachytene spermatocytes. Indeed, this was the case. We found that in *Maps*$^{-/-}$ spermatocytes, ubiquitinated proteins in chromatin fractions were significantly increased. We propose that the elevated ubiquitinated proteins likely have contributed to the dramatic dysregulation of gene expression from both sex chromosomes and autosomes, ultimately leading to male infertility. In summary, we propose that MAPS is of great importance for controlling diverse processes involved in the proper pachytene progression in spermatocytes. Since MAPS does not contain any predicted functional motif, it appears to affect protein ubiquitination through a novel mechanism. Further studies are needed to test the hypothesis that MAPS affects cellular proteolysis pathway in spermatocytes and to understand why MAPS plays such essential roles in mammalian meiosis.

Nonobstructive azoospermia (NOA) patients carrying loss-of-function mutations of meiosis-related genes have been reported to show spermatocyte development arrest. This condition has been linked to mutations in the meiosis genes, such as *TEX11* (testis expressed 11) and *SYCP3* (40, 41). It will be interesting to determine whether mutations in *MAPS* can also lead to NOA or similar conditions. Future studies to reveal whether MAPS has a role in the epigenetic controls of human spermatogenesis is also a subject of interest for the diagnosis and potential treatment of certain types of male infertility.

Methods

The *Maps*$^{-/-}$ mouse model in a C57BL/6 genetic background was generated by Cyagen Biosciences by deleting an 1,841-bp genomic DNA fragment spanning exon 3 using the CRISPR/Cas9-mediated genome-editing system (*SI Appendix*, Fig. S2*A*). The founder mice were genotyped by PCR and DNA sequencing analysis of DNA extracted from mouse tails. One selected F0 founder mouse was bred to wild-type mice to obtain F1 heterozygous mutant (*Maps*$^{+/-}$) mice, and the *Maps*$^{+/-}$ mice were used to backcross to C57/B6 wild-type mice to get rid of possible off-target mutations. Breeding pairs of *Maps*$^{+/-}$ male and female mice were used for obtaining wild-type (*Maps*$^{+/+}$) and homozygous-deficient (*Maps*$^{-/-}$) mice. Additional details and the characterization of the *Maps*$^{-/-}$ mice and the *Maps* knock-in mice, as well as all other materials and methods, are described in detail in *SI Appendix, Methods*.

Data Availability. All study data are included in the article and/or *SI Appendix*.

ACKNOWLEDGMENTS. This work was supported by grants from the Hong Kong Research Grant Council (to K.L. and R.H.W.L.), the Sanming Project of Medicine in Shenzhen, China (SZSM201612083), Shenzhen–Hong Kong Innovation Circle Type D (to K.L.), Shenzhen Science and Technology Program (KQTD20190929172749226 to W.S.B.Y. and K.L.), The University of Hong Kong-Shenzhen Hospital Fund for Shenzhen Key Medical Discipline (SZXK2020089), the High Level-Hospital Program, Health Commission of Guangdong Province, China (HKUSZH201902018 to K.L.), the National Key R&D Program of China (2018YFE0201101 to C.H.), the National Natural Science Foundation of China (to K.L. and M.L.), the National Institute of Health (R01 GM130696 to H.W.), and the Anderson Family Endowment Fund (to L.T.C.). We thank several technicians for their kind contributions to this project. We also thank various colleagues and researchers for constructive discussions.

1. S. Keeney, C. N. Giroux, N. Kleckner, Meiosis-specific DNA double-strand breaks are catalyzed by Spo11, a member of a widely conserved protein family. *Cell* **88**, 375–384 (1997).
2. M. S. Wold, Replication protein A: A heterotrimeric, single-stranded DNA-binding protein required for eukaryotic DNA metabolism. *Annu. Rev. Biochem.* **66**, 61–92 (1997).
3. K. Yoshida *et al.*, The mouse RecA-like gene Dmc1 is required for homologous chromosome synapsis during meiosis. *Mol. Cell* **1**, 707–718 (1998).
4. A. Shinohara, H. Ogawa, T. Ogawa, Rad51 protein involved in repair and recombination in *S. cerevisiae* is a RecA-like protein. *Cell* **69**, 457–470 (1992).
5. G. V. Börner, N. Kleckner, N. Hunter, Crossover/noncrossover differentiation, synaptonemal complex formation, and regulatory surveillance at the leptotene/zygotene transition of meiosis. *Cell* **117**, 29–45 (2004).
6. B. D. McKee, M. A. Handel, Sex chromosomes, recombination, and chromatin conformation. *Chromosoma* **102**, 71–80 (1993).
7. J. M. Turner, Meiotic sex chromosome inactivation. *Development* **134**, 1823–1831 (2007).
8. G. S. Roeder, J. M. Bailis, The pachytene checkpoint. *Trends Genet.* **16**, 395–403 (2000).
9. F. Baudat, Y. Imai, B. de Massy, Meiotic recombination in mammals: Localization and regulation. *Nat. Rev. Genet.* **14**, 794–806 (2013).
10. M. A. Handel, J. C. Schimenti, Genetics of mammalian meiosis: Regulation, dynamics and impact on fertility. *Nat. Rev. Genet.* **11**, 124–136 (2010).
11. V. V. Subramanian, A. Hochwagen, The meiotic checkpoint network: Step-by-step through meiotic prophase. *Cold Spring Harb. Perspect. Biol.* **6**, a016675 (2014).
12. D. Zickler, N. Kleckner, Recombination, pairing, and synapsis of homologs during meiosis. *Cold Spring Harb. Perspect. Biol.* **7**, a016626 (2015).
13. U. Schlecht *et al.*, Expression profiling of mammalian male meiosis and gametogenesis identifies novel candidate genes for roles in the regulation of fertility. *Mol. Biol. Cell* **15**, 1031–1043 (2004).
14. M. Wang *et al.*, Single-cell RNA sequencing analysis reveals sequential cell fate transition during human spermatogenesis. *Cell Stem Cell* **23**, 599–614.e4 (2018).
15. R. Bose, G. Manku, M. Culty, S. S. Wing, Ubiquitin-proteasome system in spermatogenesis. *Adv. Exp. Med. Biol.* **759**, 181–213 (2014).
16. H. B. Rao *et al.*, A SUMO-ubiquitin relay recruits proteasomes to chromosome axes to regulate meiotic recombination. *Science* **355**, 403–407 (2017).
17. W. M. Baarends *et al.*, Histone ubiquitination and chromatin remodeling in mouse spermatogenesis. *Dev. Biol.* **207**, 322–333 (1999).
18. X. L. Wu *et al.*, The testis-specific gene 1700102P08Rik is essential for male fertility. *Mol. Reprod. Dev.* **87**, 231–240 (2020).
19. M. Li *et al.*, The histone modification reader ZCWPW1 is required for meiosis prophase I in male but not in female mice. *Sci. Adv.* **5**, eaax1101 (2019).
20. H. Gan *et al.*, Dynamics of 5-hydroxymethylcytosine during mouse spermatogenesis. *Nat. Commun.* **4**, 1995 (2013).
21. M. Li *et al.*, The novel male meiosis recombination regulator coordinates the progression of meiosis prophase I. *J. Genet. Genomics* **47**, 451–465 (2020).
22. Z. Tu *et al.*, Speedy A-Cdk2 binding mediates initial telomere-nuclear envelope attachment during meiotic prophase I independent of Cdk2 activation. *Proc. Natl. Acad. Sci. U.S.A.* **114**, 592–597 (2017).

23. Z. Xue, D. Xu, Y. Wang, Y. Zhang, ThreaDom: Extracting protein domain boundary information from multiple threading alignments. *Bioinformatics* **29**, i247–i256 (2013).
24. A. Inselman, S. Eaker, M. A. Handel, Temporal expression of cell cycle-related proteins during spermatogenesis: Establishing a timeline for onset of the meiotic divisions. *Cytogenet. Genome Res.* **103**, 277–284 (2003).
25. Y. Clermont, Kinetics of spermatogenesis in mammals: Seminiferous epithelium cycle and spermatogonial renewal. *Physiol. Rev.* **52**, 198–236 (1972).
26. C. A. Hogarth *et al*., Processive pulses of retinoic acid propel asynchronous and continuous murine sperm production. *Biol. Reprod.* **92**, 37 (2015).
27. S. Sigismund, S. Polo, P. P. Di Fiore, Signaling through monoubiquitination. *Curr. Top. Microbiol. Immunol.* **286**, 149–185 (2004).
28. V. Chau *et al*., A multiubiquitin chain is confined to specific lysine in a targeted short-lived protein. *Science* **243**, 1576–1583 (1989).
29. V. A. Tillu, O. Kovtun, K. A. McMahon, B. M. Collins, R. G. Parton, A phosphoinositide-binding cluster in cavin1 acts as a molecular sensor for cavin1 degradation. *Mol. Biol. Cell* **26**, 3561–3569 (2015).
30. S. Jackson, Y. Xiong, CRL4s: The CUL4-RING E3 ubiquitin ligases. *Trends Biochem. Sci.* **34**, 562–570 (2009).
31. L. A. Higa, H. Zhang, Stealing the spotlight: CUL4-DDB1 ubiquitin ligase docks WD40-repeat proteins to destroy. *Cell Div.* **2**, 5 (2007).
32. P. Goetz, A. C. Chandley, R. M. Speed, Morphological and temporal sequence of meiotic prophase development at puberty in the male mouse. *J. Cell Sci.* **65**, 249–263 (1984).
33. W. Edelmann *et al*., Meiotic pachytene arrest in MLH1-deficient mice. *Cell* **85**, 1125–1134 (1996).
34. O. Fernandez-Capetillo *et al*., H2AX is required for chromatin remodeling and inactivation of sex chromosomes in male mouse meiosis. *Dev. Cell* **4**, 497–508 (2003).
35. Y. Ichijima *et al*., MDC1 directs chromosome-wide silencing of the sex chromosomes in male germ cells. *Genes Dev.* **25**, 959–971 (2011).
36. T. Hirota *et al*., SETDB1 links the meiotic DNA damage response to sex chromosome silencing in mice. *Dev. Cell* **47**, 645–659.e6 (2018).
37. K. J. Grive *et al*., Dynamic transcriptome profiles within spermatogonial and spermatocyte populations during postnatal testis maturation revealed by single-cell sequencing. *PLoS Genet.* **15**, e1007810 (2019).
38. S. Yoshida *et al*., The first round of mouse spermatogenesis is a distinctive program that lacks the self-renewing spermatogonia stage. *Development* **133**, 1495–1505 (2006).
39. M. J. Zelazowski *et al*., Age-dependent alterations in meiotic recombination cause chromosome segregation errors in spermatocytes. *Cell* **171**, 601–614.e13 (2017).
40. F. Yang *et al*., TEX11 is mutated in infertile men with azoospermia and regulates genome-wide recombination rates in mouse. *EMBO Mol. Med.* **7**, 1198–1210 (2015).
41. T. Miyamoto *et al*., Azoospermia in patients heterozygous for a mutation in SYCP3. *Lancet* **362**, 1714–1719 (2003).